Supporting Information

Synergistic hydrazine-driven regulation and Mo/S co-doping to endow BiOBr with heterovalent molybdenum states and abundant oxygen vacancy defects for photocatalytic hydrogen evolution

Zhengjie Su[1], Binghong Wu[1], Dong-Hau Kuo[2,*], Longyan Chen[1], Pengkun Zhang[1], Baoqian Yang[1], Xinru Wu[1], Dongfang Lu[1,*], Jinguo Lin[1,*], Xiaoyun Chen[1,*]

[1] College of Materials Engineering, Fujian Agriculture and Forestry University, Fuzhou 350002, China

[2] Department of Materials Science and Engineering, National Taiwan University of Science and Technology, Taipei 10607, Taiwan

*Corresponding author

E-mail address: dhkuo@mail.ntust.edu.tw (D. H. Kuo)

E-mail address: fjldf@126.com (D. Lu)

E-mail address: fjlinjg@126.com (J. Lin)

E-mail address: fjchenxy@126.com (X. Chen)

Experimental Section

1. Apparent quantum efficiency computation

According to the literature reports [1-2] for measuring the apparent quantum efficiency (AQE). The experiment was measured under the photocatalytic reaction conditions of monochromatic light of 420 nm (λ), average radiation intensity (I) of 3.23 mW/cm^{-2}, and irradiation area (A) of 31.9 cm^2. The total H_2 evolution with 50 mg of Mo/S-BiOBr-3 catalyst was 543.8 μmol, which can be used to determine the reacted photons (N_{reac}). The number of photons (N_{in}) illuminated to the reactor is computed according to the following equations:

$$N_{in} = \frac{E \times \lambda}{h \times c} = \frac{A \times I \times t \times \lambda}{h \times c} = \frac{31.9 \times 3.23 \times 10^{-3} \times 3600 \times 6 \times 420 \times 10^{-9}}{6.626 \times 10^{-34} \times 3 \times 10^{8}} = 4.72 \times 10^{21}$$

$$AQE = \frac{N_{reac}}{N_{in}} \times 100\% = \frac{2 \times 6.02 \times 10^{23} \times 543.8 \times 10^{-6}}{4.72 \times 10^{21}} \times 100\ \% = 13.9\ \%$$

Additional figures and tables

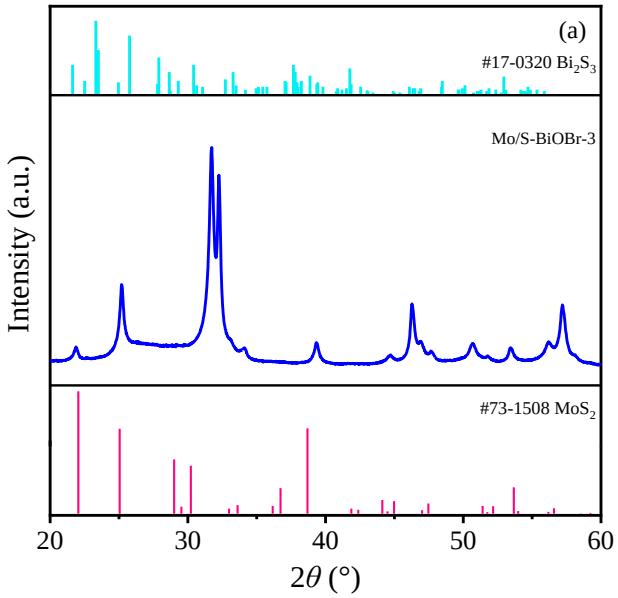

Fig. S1 XRD pattern of Mo/S-BiOBr-3 with the Bi_2S_3 (PDF #17-0320) and MoS_2 (PDF #73-1508) standard cards.

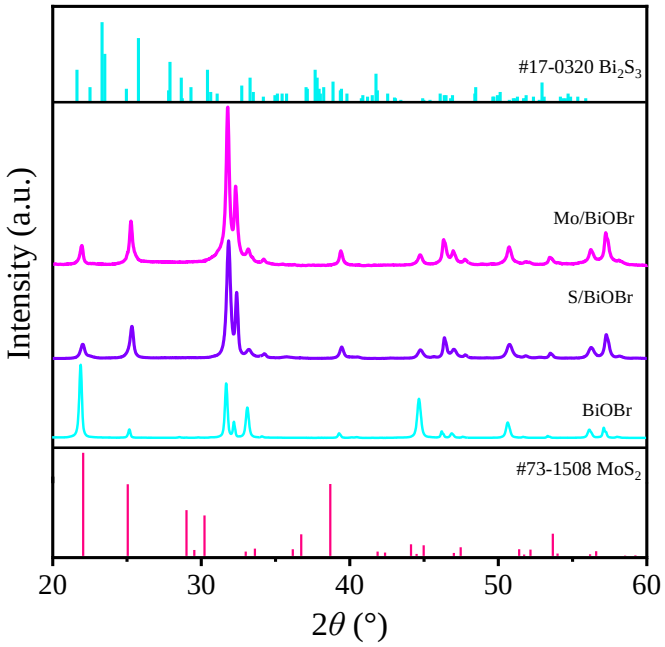

Fig. S2 XRD patterns of BiOBr, Mo/BiOBr, and S/BiOBr with the Bi_2S_3 (PDF #17-0320) and MoS_2 (PDF #73-1508) standard cards.

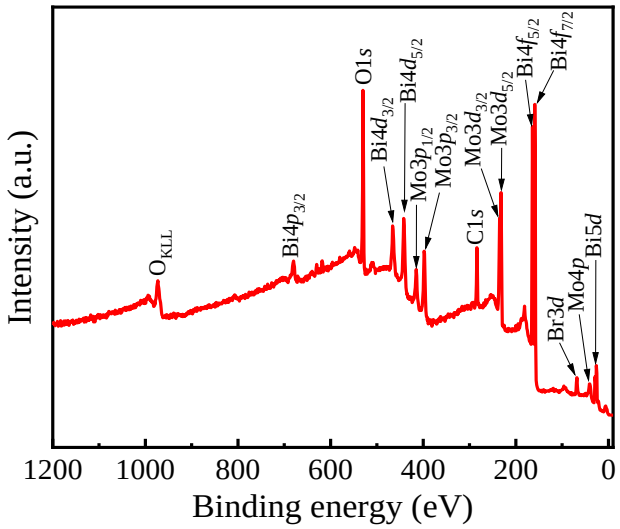

Fig. S3 The survey XPS spectrum of Mo/S-BiOBr-3.

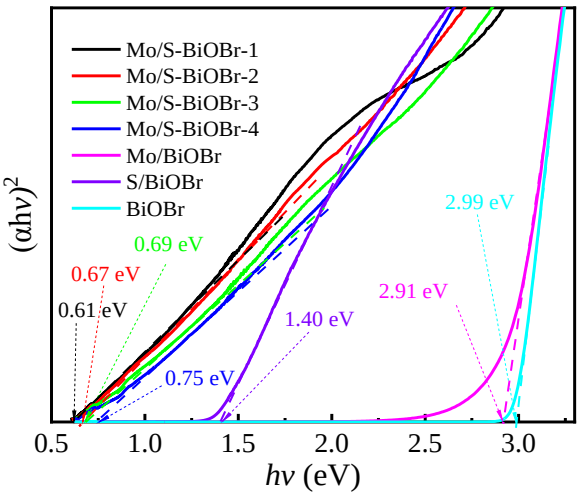

Fig. S4 The direct bandgap $(\alpha h\nu)^2$ - *hν* curves of Mo/S-BiOBr, Mo/BiOBr, S/BiOBr, and BiOBr catalysts.

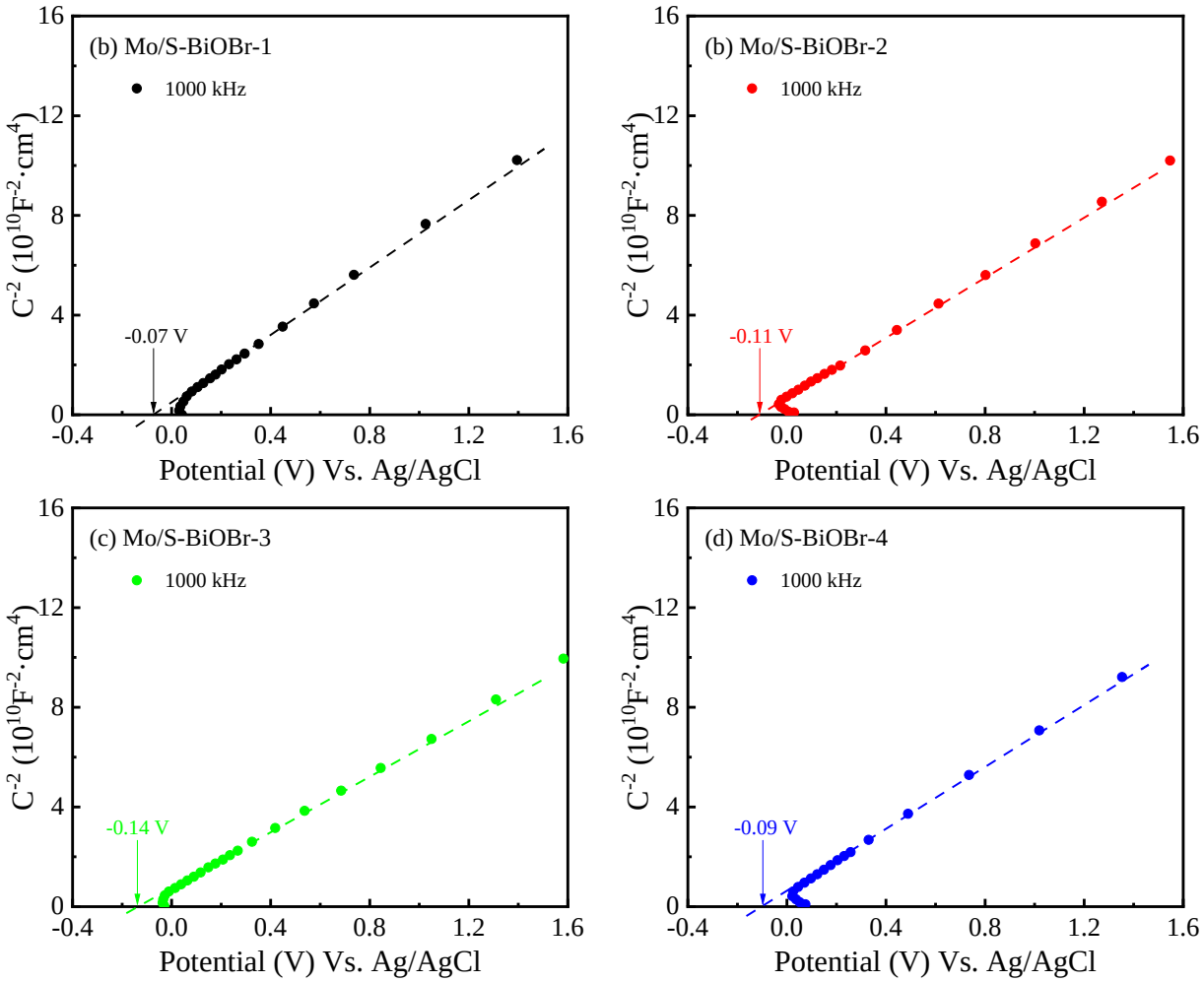

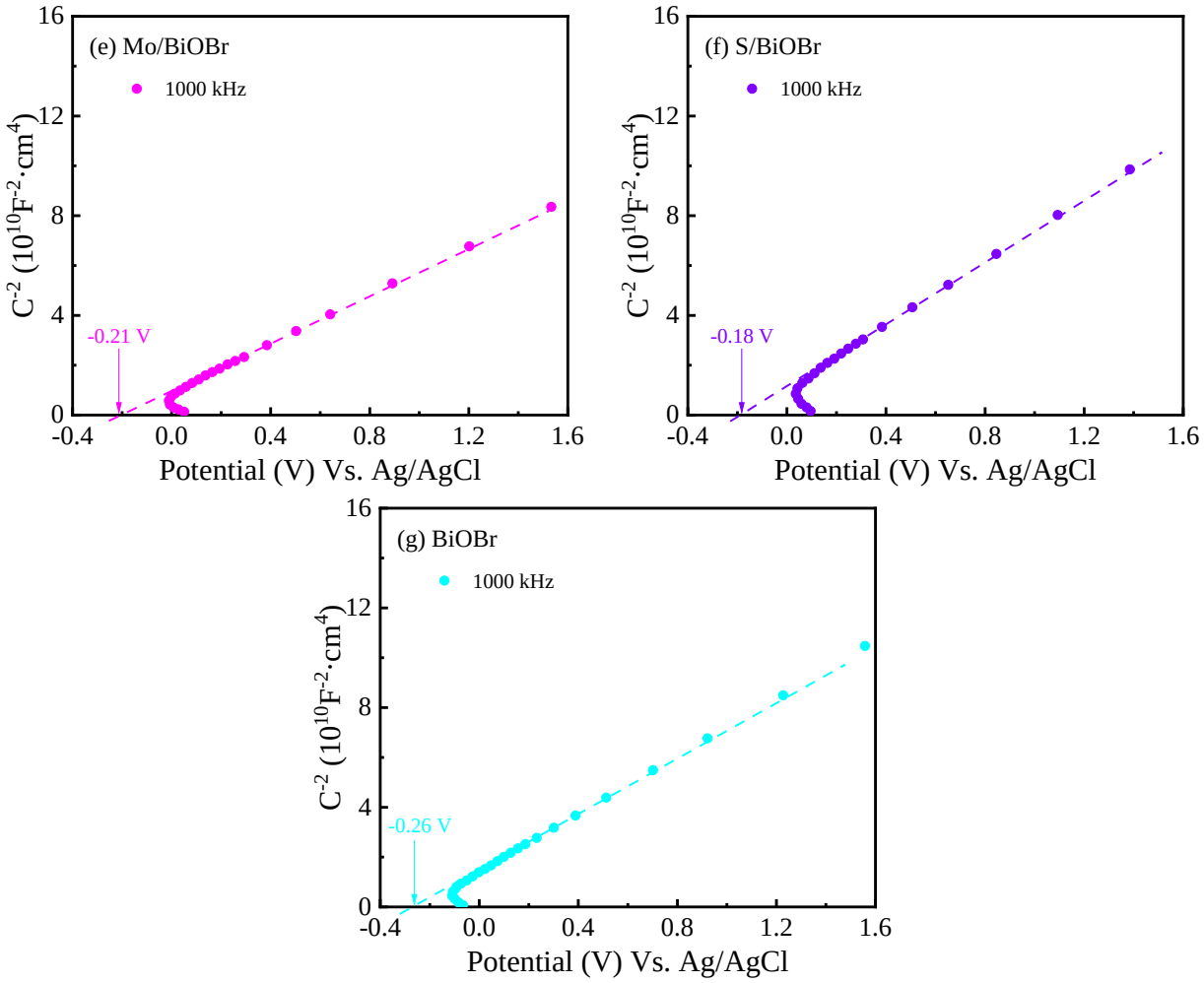

Fig. S5 Mott-Schottky curves of Mo/S-BiOBr, Mo/BiOBr, and S/BiOBr at 1000 kHz.

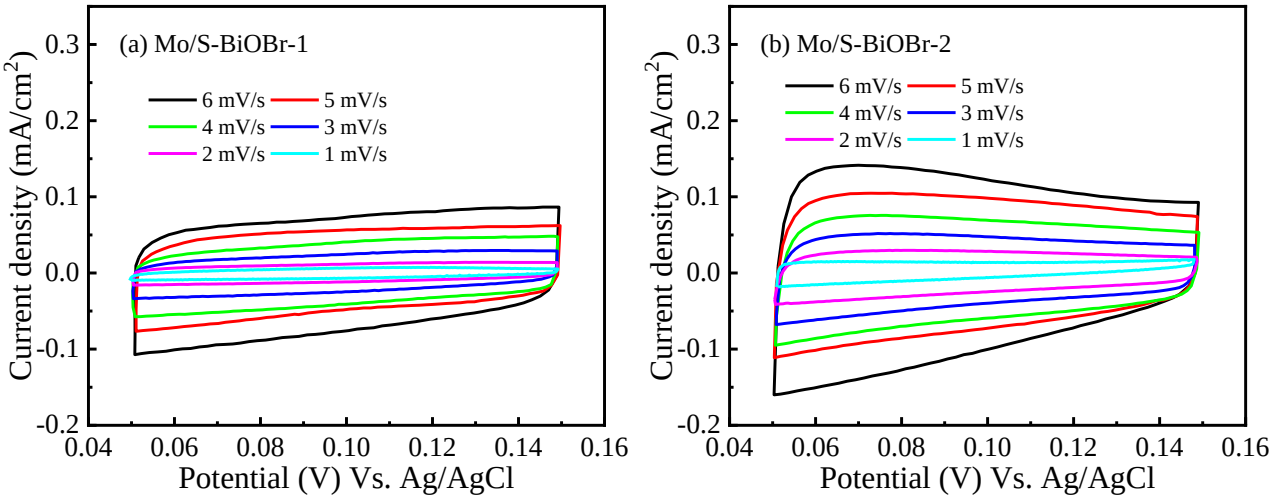

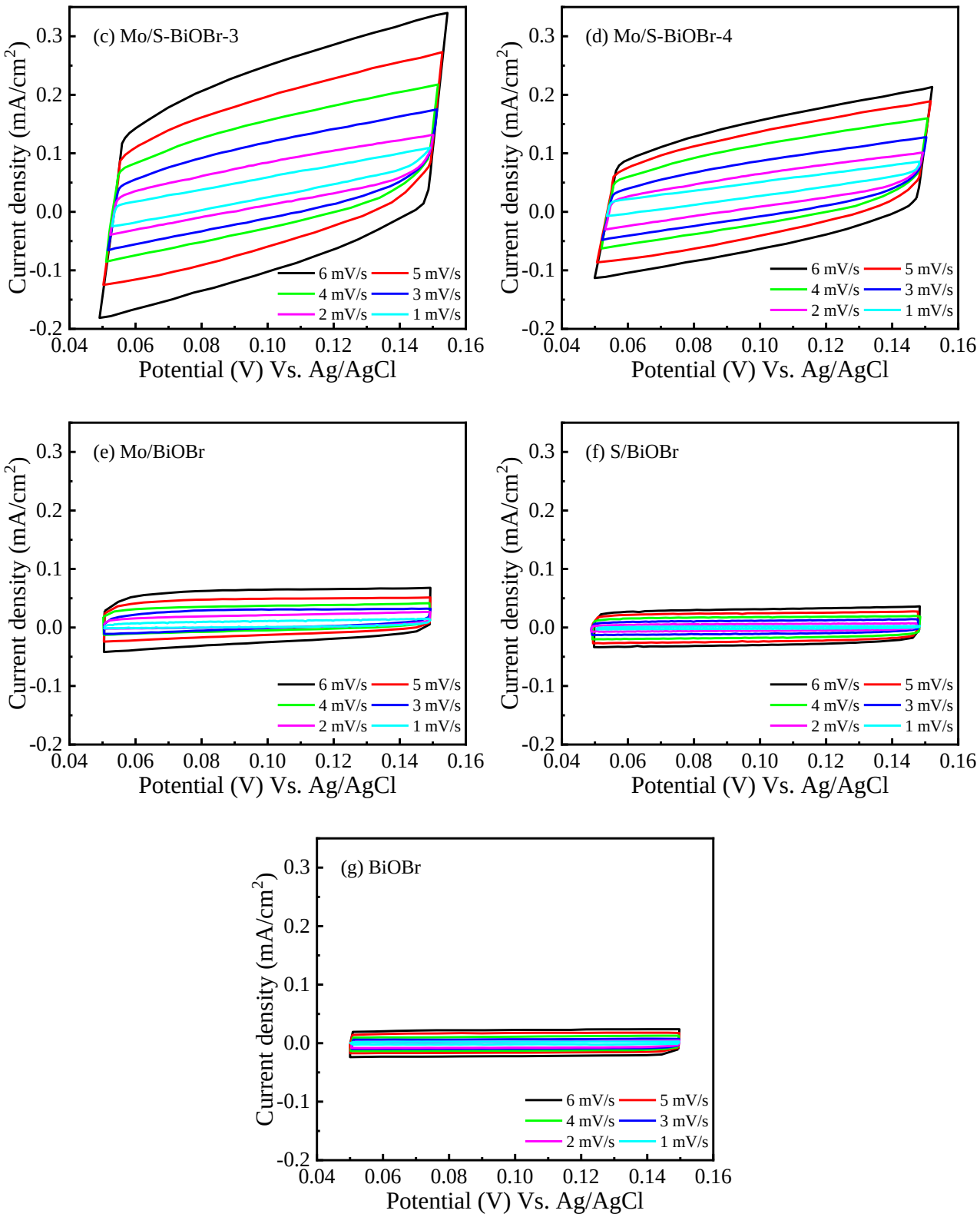

Fig. S6 Current density-potential plots of (a) Mo/S-BiOBr-1, (b) Mo/S-BiOBr-2, (c) Mo/S-BiOBr-3, (d) Mo/S-BiOBr-4, (e) Mo/BiOBr, (f) S/BiOBr, and (g) BiOCl.

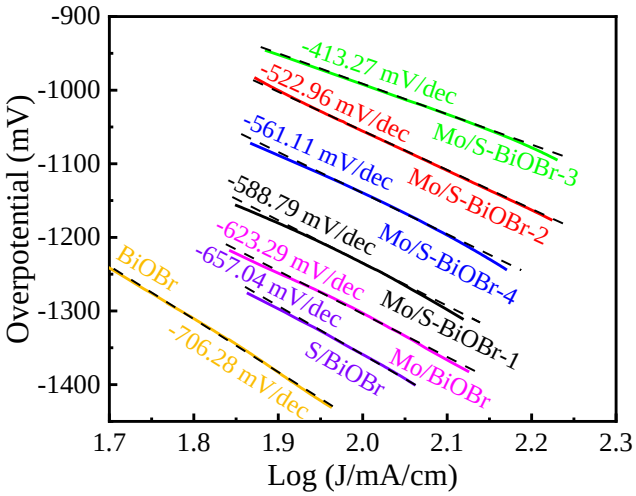

Fig. S7 Tafel-slope plots of Mo/S-BiOBr, Mo/BiOBr, S/BiOBr, and BiOBr electrocatalysts.

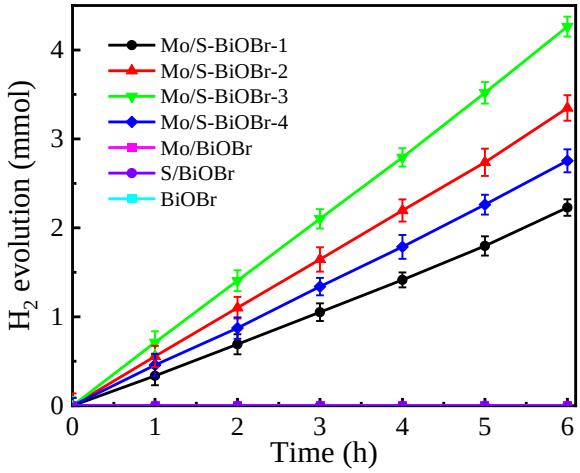

Fig. S8 Photocatalytic hydrogen evolution of BiOBr-based catalysts varied with the duration time.

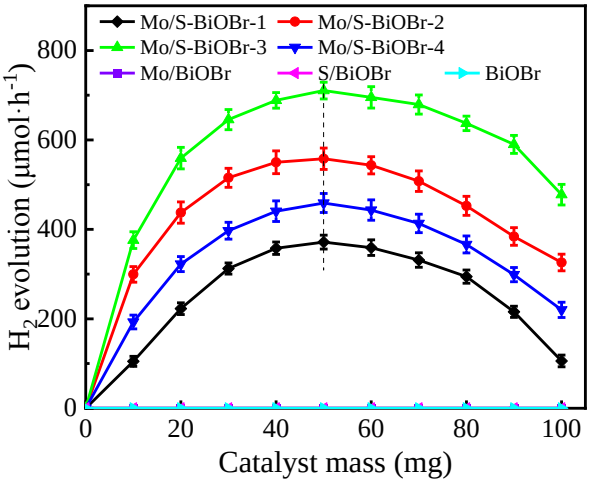

Fig. S9 Variation of PHER rate with the amount of Mo/S-BiOBr, Mo/BiOBr, S/BiOBr, and BiOBr catalysts.

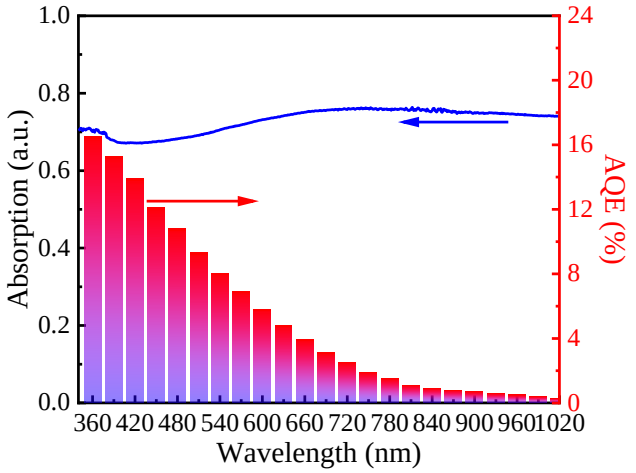

Fig. S10 Dependence of AQE Mo/S-BiOBr-3 as a function of irradiation wavelength, combining the UV−vis absorption spectrum.

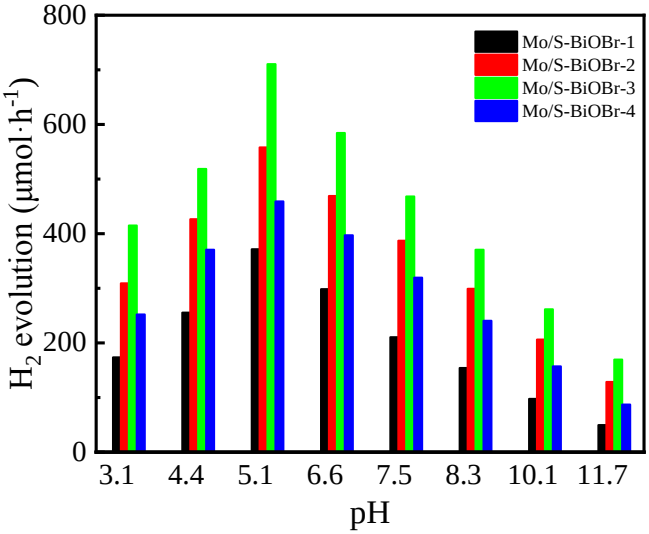

Fig. S11 PHER of Mo/S-BiOBr at different pH values.

Table S1 XPS composition, V_O (%), crystal size, and S_{BET} analyses of Mo/S-BiOBr and BiOBr catalysts

Catalyst	Atomic percentage/%					$Mo^{4+}/Mo^{4+}+Mo^{6+}$ (%)	V_O (%)	Crystallinity (%)	Crystal size (nm)	S_{BET} ($m^2 \cdot g^{-1}$)	Pore volume ($cm^3 \cdot g^{-1}$)
	Bi	Mo	Br	S	O						
Mo/S-BiOBr-1	27.83	6.47	23.31	8.21	34.18	29.73	7.11	90.48	45.7	14.1	0.148
Mo/S-BiOBr-2	28.09	6.51	22.96	8.11	34.33	32.64	12.75	89.97	30.0	15.5	0.161
Mo/S-BiOBr-3	27.76	6.39	23.17	8.15	34.53	37.40	18.50	90.52	18.2	16.3	0.186
Mo/S-BiOBr-4	27.98	6.42	23.13	8.19	34.28	41.58	9.96	89.83	15.4	14.8	0.159
BiOBr	32.77	N/A	30.40	N/A	36.83	N/A	N/A	94.99	63.8	0.1	0.017
Mo/S-BiOBr-3 after reaction	27.68	6.45	22.99	8.09	34.79	37.26	18.44	89.94	19.1	15.9	0.181

Table S2 Element contents from SEM-EDS analysis for Mo/S-BiOBr and BiOBr catalysts

Catalyst	Bi	Mo	Br	S	O
Mo/S-BiOBr-1	27.63	6.39	23.27	8.39	34.32
Mo/S-BiOBr-2	27.97	6.43	23.06	8.14	34.40
Mo/S-BiOBr-3	27.84	6.47	22.98	8.11	34.60
Mo/S-BiOBr-4	28.07	6.33	23.07	8.14	34.39
BiOBr	32.84	N/A	30.43	N/A	36.73

Table S3 XRF chemical element compositions of Mo/S-BiOBr and BiOBr catalysts

Catalyst	Bi	Mo	Br	S	O
Mo/S-BiOBr-1	27.73	6.43	23.34	8.27	34.23
Mo/S-BiOBr-2	28.11	6.33	23.03	8.19	34.34
Mo/S-BiOBr-3	27.81	6.41	23.12	8.08	34.58
Mo/S-BiOBr-4	27.93	6.45	23.10	8.21	34.31
BiOBr	32.92	N/A	30.38	N/A	36.70

Table S4 Reports on PHER performance over bismuth oxyhalide catalysts under visible light

Catalyst	Sacrificial agent	Light source	AQE/AQY (%)	PHER rate ($mmol \cdot g^{-1} \cdot h^{-1}$)	Refs.
BiOBr/$W_{18}O_{49}$/PAN	1 wt% H_2PtCl_6	300 W Xe	N/A	0.95×10^{-3}	[3]
BiOBr/$Bi_{24}O_{31}Br_{10}$/Ti_3C_2	triethanolamine	500 W Me	N/A	1.25×10^{-2}	[4]
CQDs/Bi_2WO_6/BiOBr	triethanolamine	350 W Xe	AQY 1.05 (350 nm)	0.46	[5]
BiOBr/$ZnIn_2S_4$	10 vol% TEOA	300 W Xe	AQE 1.6 (420 nm)	0.69	[6]
O/D-Bi_5O_7Br	40 vol% CH_3OH	300 W Xe	N/A	0.38×10^{-2}	[7]
I-BiOBr/g-C_3N_4	TEOA	300 W Xe	N/A	0.31	[8]
α-Fe2O3/BiOBr/g-C3N4	CIP/LVX	300 W Xe	N/A	2.57	[9]
Bi_3O_4Br	10 vol% methanol	300 W Xe	N/A	0.38	[10]
$Bi_4O_5Br_2$	40 vol% methanol	300 W Xe	AQE 0.93 (420 nm)	0.17	[11]
$Bi_{24}O_{31}Br_{10}$	10 vol% methanol	300 W Xe	N/A	0.06	[12]
AgI-BiOI	Na_2S/NaCl/Na_2SO_3	300 W Xe	N/A	0.168	[13]
BiOCl/WO_3	TEOA	300 W Xe	N/A	0.084	[14]
K-BiOI	Methanol	300 W Xe	N/A	6.51	[15]
BiOCl/TiO_2	TEOA	300 W Xe	N/A	1.35	[16]
BiOI@BiOI	Methanol	300 W Xe	N/A	0.048	[17]
CdS-BiOCl/PAN	Lactic acid	300 W Xe	N/A	0.288	[18]
Mo/S-BiOBr	Na_2S/Na_2SO_3	300 W Xe	AQE 13.9 (420 nm)	9.46	This work

Table S5 The photocatalytic hydrogen evolution in terms of the $Mo^{4+}/(Mo^{4+}+Mo^{6+})$ (%) and Vo (%) values for BiOBr, Mo/BiOBr, S/BiOBr, and Mo/S-BiOBr catalysts

	H_2 ($mmol \cdot g^{-1} \cdot h^{-1}$)	$Mo^{4+}/(Mo^{4+}+Mo^{6+})$ (%)	Vo (%)
BiOBr	0	0	0
Mo/BiOBr	0	0	0
S/BiOBr	0	0	0
Mo/S-BiOBr-1	7.43	29.73	7.11
Mo/S-BiOBr-2	11.16	32.64	12.75
Mo/S-BiOBr-3	14.21	37.40	18.50
Mo/S-BiOBr-4	9.18	41.58	9.96

Reference:

[1] C. Imparato, G. Iervolino, M. Fantauzzi, C. Koral, W. Macky, M. Kobielusz, G. D'Errico, I. Rea, R.D. Girolamo, L.D. Stefano, A. Andreone, V. Vaiano, A. Rossi, A. Aronne, Photocatalytic hydrogen evolution by cocatalyst free TiO_2/C bulk heterostructures synthesized under mild conditions, *RSC Adv.*, 10 (2020) 12519–12534.

[2] M.S. Nasir, G. Yang, I. Ayub, S. Wang, W. Yan, Tin diselinide a stable co-catalyst coupled with branched TiO_2 fiber and g-C_3N_4 quantum dots for photocatalytic hydrogen evolution, *Appl. Catal. B-Environ.*, 270 (2020) 118900.

[3] Y. Wang, R. Tao, T. Yan, T. Li, X. Fan, Z. Chu, K. Liu, Construction of flexible BiOBr/$W_{18}O_{49}$/polyacrylonitrile discrete heterojunction nanofibers as a dual-functional photocatalyst for simultaneous hydrogen evolution and organic pollutant degradation, *Colloids Surf. A: Physicochem. Eng. Aspects*, 694 (2024) 134054.

[4] L. Zhang, J. Song, X. Meng, W. Liu, Bismuth-rich BiOBr/$Bi_24O_{31}Br_{10}$/Ti_3C_2 polyheterojunction for visible photocatalytic degradation of dyes and Cr(VI) reduction and hydrogen production applications, *J. Alloys Compd.*, 997 (2024) 174873.

[5] Y. Zhang, Y. Li, Y. Yuan, S-scheme BiOBr/Bi_2WO_6 with oxygen vacancies for synergistic photodegradation and hydrogen generation: Mechanisms insight and DFT calculations, *J. Alloys Compd.*, 995 (2024) 174755.

[6] X. Kuang, X. Jin, F. Chen, A. Pan, H. Duan, Z. Wu, B. Cao, Construction of the V_OBiOBr/$V_S$$ZnIn_2S_4$ heterojunction for photocatalytic hydrogen production and dye removal under simulated sunlight, *Int. J. Hydrogen Energy*, 74 (2024) 361–371.

[7] F. Xie, L. Zhang, X. Zhang, M. Zhang, X. Jian, J. Liu, X. Zhang, Y. Wang, R. Li, C. Fan,

Enhancement of visible light photocatalytic pharmaceutical degradation and hydrogen evolution of Bi_5O_7Br by in situ disorder engineering, *T. Nonferr. Metal. Soc.*, 33 (2023) 1862–1872.

[8] W. Li, X. Ruan, Z. Wei, S. Lian, X. Cui, J. Wang, Tuned band structure and *H reduction pathway of photocatalytic performance towards I-BiOBr/g-C_3N_4 heterostructure, *Energy Technol.*, 11 (2023) 2201100.

[9] Z. Wang, M. Dou, X. Liu, S. Kang, L. Kong, H. Yang, Y. Zhang, Y. Chen, H. Zhu, J. Dou, Ternary Z-scheme α-Fe_2O_3/BiOBr/g-C_3N_4 photocatalyst for highly efficient hydrogen production coupled with diverse antibiotic degradation, *J. Environ. Chem. Eng.*, 12 (2024) 113080.

[10] J. Di, J. Xia, M.F. Chisholm, J. Zhong, C. Chen, X. Cao, F. Dong, Z. Chi, H. Chen, Y. Weng, J. Xiong, S. Yang, H. Li, Z. Liu, S. Dai, Defect-tailoring mediated electron-hole separation in single-unit-cell Bi_3O_4Br nanosheets for boosting photocatalytic hydrogen evolution and nitrogen fixation, *Adv. Mater.*, 31 (2019) 1807576.

[11] Y. Bai, T. Chen, P. Wang, L. Wang, L. Ye, Bismuth-rich $Bi_4O_5X_2$ (X = Br, and I) nanosheets with dominant {101} facets exposure for photocatalytic H_2 evolution, *Chem. Eng. J.*, 304 (2016) 454–460.

[12] J. Shang, W. Hao, X. Lv, T. Wang, X. Wang, Y. Du, S. Dou, T. Xie, D. Wang, J. Wang, Bismuth oxybromide with reasonable photocatalytic reduction activity under visible light, *ACS Catal.*, 4 (2014) 954–961.

[13] C.-J. Chang, Y.-G. Lin, P.-Y. Chao, J.-K. Chen, AgI-BiOI-graphene composite photocatalysts with enhanced interfacial charge transfer and photocatalytic H_2 production activity, *Appl. Surf. Sci.*, 469 (2019) 703–712.

[14] D. Sun, M. Zhang, L. Huang, Y. Qu, Y. Yu, B. Lou, H. Du, B. Xu, K. Wang, Intermediate products driven one-pot in-situ synthesis of BiOCl/WO_3 heterojunction with enhanced photocatalytic

hydrogen and oxygen evolution for potential industrial applications, *J. Alloys Compd*., 969 (2023) 172433.

[15] J. Yang, H. Su, Y. Wu, D. Li, D. Zhang, H. Sun, S. Yin, Facile synthesis of kermesinus BiOI with oxygen vacancy for efficient hydrogen generation, *Chem. Eng. J.*, 420 (2021) 127607.

[16] R. Hou, M. Xu, Z. Fan, R. Zhong, Y. Xie, Y. Ling, Y. Wang, BiOCl modified TiO_2 based catalyst with enhanced hydrogen generation properties under visible light via promote photogenerated electron-hole separation. *Mater. Today Phys.*, 44 (2024) 101426.

[17] H. Huang, K. Xiao, X. Du, Y. Zhang, Vertically aligned nanosheets-array-like BiOI homojunction: Three-in-one promoting photocatalytic oxidation and reduction abilities, *ACS Sustain. Chem. Eng*., 5 (2017) 5253–5264.

[18] Q. Zhang, G. Li, J. Bai, R. He, C. Li, Enhanced photocatalytic activities of CdS-BiOCl/PAN composites towards photocatalytic hydrogen evolution, *Mater. Res. Bull*., 117 (2019) 9–17.